

ELECTRON INDUCED DESORPTION OF GASES FROM ALUMINUM*

E. L. Garwin, E. W. Hoyt,
M. Rabinowitz and J. Jurow

Stanford Linear Accelerator Center
Stanford University, Stanford, California

Paper to be presented at the Fourth International Vacuum
Congress, April 17-20, 1968, Manchester, England.

* Work supported by the U. S. Atomic Energy Commission

Electron Induced Desorption of Gases From Aluminum*

E. L. GARWIN, E. W. HOYT,
M. RABINOWITZ, and J. JUROW

Stanford Linear Accelerator Center
Stanford University, Stanford, California

Abstract

The electronic desorption of CO and its readsorption on aluminum (natural oxide film) was studied and found to be influenced by the adsorption of H₂.

A theoretical model was developed which fits the experimental data and reliably predicts the adsorption-desorption characteristics at low electron energies (100 - 300 eV). At higher energies the picture is complicated by the release of subsurface gases identified as such by using CO¹⁸ techniques.

(Paper to be presented at the Fourth International Vacuum Congress, April 17-20, 1968, Manchester, England.)

* Work supported by the U. S. Atomic Energy Commission

I. Introduction

In designing an ultra-high vacuum system for an electron-positron storage ring, it is of crucial importance to predict (and minimize) the gas produced when synchrotron radiation from circulating beams strikes the chamber wall. It is established [Plumlee and Smith (1950), Moore and Hughes (1955), Degras, Petermann and Schram (1962), Petermann (1963), Redhead (1964), Clausing (1965), Fischer and Mack (1965), Bernardini and Malter (1965), Lichtman and McQuistan (1965)], that low energy electrons can be quite efficient in removing adsorbed gas, both as ions and neutrals. Photoelectron induced desorption plays the primary role in accounting for the observed pressure increases measured in existing storage rings [O'Neill (1966)]. Our interest in aluminum arises from the need for a good thermal conductor to intercept the high-energy density synchrotron radiation striking the chamber wall, which in the case of the proposed 3-BeV e^-, e^+ [SLAC (1966)] ring, can be as high as 2.5 kilowatts per square centimeter. This photon flux produces $\sim 10^{18}$ photoelectron/cm² - sec in the 1 mm high band where it intersects the chamber walls. Under high coverage surface conditions the normal thermal desorption rate of $\sim 10^7$ molecules/cm² - sec could increase to $\sim 10^{14}$ molecules/cm² - sec under synchrotron bombardment.

A summary of our studies of electron desorbed gases from aluminum is reported here. More detailed results will be published later.

II. Experimental System

Desorption measurements on aluminum were made with the simple diode system and appendage quadrupole mass spectrometer shown schematically in Fig. 1. The tungsten filament was maintained axial by means of a tungsten weight hung from the bottom. The filament region near the flanges and feed-throughs was shielded with molybdenum (at filament potential) to prevent electron bombardment of surfaces

other than the desired region of the aluminum tube inner surface. The target tube temperature could be controlled between 77° and 500° K. However, only the room temperature results will be described here. By adjusting the filament temperature and potential, the target surface could be bombarded at electron energies from 5 eV to 16 KeV at current densities of 0.1 to $100 \mu\text{A}/\text{cm}^2$.

Following bakeout, total pressures less than 1×10^{-10} torr were routinely attained. Total pressure was measured with a trigger discharge gauge (TDG). Partial pressures were measured with a quadrupole mass filter having a detection limit of about 10^{-13} torr. With this arrangement it was not possible to directly measure at the aluminum surface the desorbed ions and neutrals. Instead the partial pressure changes at the mass spectrometer were measured and recorded continuously. H_2 , CO and smaller amounts of CH_4 and CO_2 were observed to increase under electron bombardment (see Fig. 2).

Because of its high electron scattering cross section we concentrated our measurements on CO although, as we see later, H_2 cannot be neglected.

III. Theory and Results

A. Electron Desorption Rate

The continuity equation relating volume gas to sinks and sources of gas is:

$$\frac{V}{kT} \dot{P} = \frac{V}{kT} \frac{dP}{dt} = Aq' + Q_t + Q_l - Q_{aT} - Q_{ad} - Q_{as} - Q_P \quad (1)$$

q' : gross desorption rate in molecules/ cm^2 -sec, due to electron bombardment

Q_t : thermal desorption rate from system and target

Q_l : leak rate into the system including backstreaming from pump

Q_{aT} : adsorption rate on the target, from gas at equilibrium with the system

Q_{ad} : readsorption rate on the target from desorbed gas not yet at equilibrium

Q_{as} : adsorption rate on rest of the system from all sources

Q_p : gas flux going to the pump

When the electron beam is turned off, $q' = 0$, $Q_{ad} = 0$, and there is a discontinuity in \dot{P} . Let \dot{P}_i be the values of \dot{P} at times $t - \epsilon$ and $t + \epsilon$, $\epsilon \rightarrow 0$.

$$\text{Beam on: } \frac{V}{kT} \dot{P}_1 = Aq' + Q_t + Q_l - Q_{aT} - Q_{ad} - Q_{as} - Q_p \quad (2)$$

$$\text{Beam off: } \frac{V}{kT} \dot{P}_2 = 0 + Q_t + Q_l - Q_{aT} - 0 - Q_{as} - Q_p \quad (3)$$

Subtracting (3) from (2), and rearranging to give the net flux leaving the target due to electron bombardment:

$$q = q' - \frac{1}{A} Q_{ad} = \frac{V}{AkT} [\dot{P}_1 - \dot{P}_2] \quad (4)$$

Equation (4) defines the net electron desorption rate q independent of the pumping speed, thermal outgassing rate, etc. which may vary during the course of a desorption run.

Commonly q' is obtained either from $\frac{V}{kTA} \frac{dP}{dt}$ when the electron beam is switched on, or from $S(P - P_0)/kTA$ when dP/dt is zero or very small [Degras(1962)] However, both methods require that the total pumping speed, S , and $Q_t + Q_l$ remain constant over the range P_0 to P , which is often not true.

B. General Desorption Equations

For the i -th state being desorbed from the target surface:

$$\dot{n}_i = \frac{dn_i}{dt} = -\sigma_i j n_i + f_i \left(\frac{vP_0}{4kT} \right) + q_{b_i} - q_{b'_i} - q_{Tt_i} + a_i \sum_i \sigma_i j n_i \quad (5)$$

n_i : number of molecules per cm^2 in the i -th state on the target surface

σ_i : electron desorption cross section of a molecule in the i -th state, in cm^2

j : bombarding electron current density in $\text{electrons}/\text{cm}^2\text{-sec}$

f_i : sticking probability of a gas molecule for the i -th state

q_{b_i} : gas diffusion flux from the bulk to the target surface onto state i

q_{b_i}' : gas diffusion into the bulk from state i on the target surface

q_{Tt_i} : thermal desorption from the i -th state on the target

a_i : fraction of the desorbed molecules which are readsorbed on state i

Our surface desorption data is obtained at 100 eV bombarding energy after long periods of higher energy bombardment which renders the bulk quite gas free immediately below the surface, hence $q_b \doteq 0$. Since the target is water-cooled, and the bombarding current density is relatively high, q_b , and q_{Tt} are assumed negligible relative to the other terms. If there were only one state, Eq. (5) would take the form:

$$(5) \rightarrow \dot{n}_i = -\sigma_i j n_i (1 - a_i) + f_i \left(\frac{vP_0}{4kT} \right) \quad \text{with} \quad a_i = b_{i1} + b_{i2} - b_{i1} b_{i2} \quad (6)$$

$$b_{i1} \doteq f_i \sum_{k=0}^{N-1} (1 - f_i)^k (1 - G)^{k+1} \quad (7a) \quad \text{and} \quad b_{i2} \doteq \frac{2 \times 10^2 f_i}{1 + 2 \times 10^2 f_i} \quad (7b)$$

where N is the average number of bounces a desorbed molecule makes with the target before leaving the target region, $N \sim 5$. G is a geometrical factor for the direct escape of particles from the target region to the system, $G \doteq 0.05$.

$$\text{Let } \sigma_i^* \equiv \sigma_i (1 - a_i) \quad (8)$$

f_i is a function of n_i ; however, assuming f_i remains constant,

$$(6) \Rightarrow n_i = n_{ie} + (n_{i0} - n_{ie}) e^{-\sigma_i^* j t} \quad (9)$$

where n_{i0} is the initial coverage, and

$$n_{ie} = \frac{f_i v P_0}{4kT \sigma_i^* j} \quad \text{is the equilibrium coverage.} \quad (10)$$

$$\text{The desorption rate is } q_i = \sigma_i^* j n_i, \quad \text{and} \quad q_{ie} = \sigma_i^* j n_{ie} = f_i (v P_0 / 4kT) \quad (11)$$

is the equilibrium desorption rate when for every molecule desorbed from the target one is adsorbed.

The situation is not so simple when there is more than one state. There may be migration on the surface from one state to another, which we shall neglect. A molecule desorbed from one state may readsorb on another. This leads to a set of coupled differential equations which are quite difficult to solve. The algebraic solution limit of these equations allows us to estimate that the error may not be significant in neglecting cross-readsorption. With these assumptions, we get as a first approximation to the many-state case a linear sum of the solutions for each state:

$$q = \sum_i q_i = \sum_i q_{ie} + (q_{i0} - q_{ie}) e^{-\sigma_i^* j t}, \quad (12)$$

and similarly for n .

C. Transient Response Following Repopulation at Reduced Bombardment

Equation (6) makes an interesting prediction which seems well borne out by the experimental data. Suppose that we bombard at current density j_1 until equilibrium is reached.

$$\dot{n}_i = 0, \quad q_{ie1} = \sigma_i^* j_1 n_{ie1} = \left(\frac{v}{4kT}\right) f_i P_0 \quad (13)$$

Now reduce j to $j_2 = \frac{1}{b} j_1$. Substituting into Eq. (6) and integrating gives:

$$n_i = \left(\frac{v}{4kT}\right) \frac{f_i P_0}{\sigma_i^* j_2} \left[1 + \left(\frac{1}{b} - 1\right) e^{-\sigma_i^* j_2 t} \right]. \quad (14)$$

This says that under reduced bombardment the higher cross section states approach their new higher equilibrium populations sooner than the lower cross section states.

The repopulation is evidenced by an increase in the desorption rate signal,

$$q_{i2} = \sigma_i^* j_2 n_i \longrightarrow q_{ie1} \text{ as } t \longrightarrow \infty.$$

After some time of reduced bombardment, t_3 , j is increased back to j_1 .

Integrating Eq. (6) as before gives

$$q_{i3} = q_{ie1} - q_{ie1} \left\{ 1 - \left[b - (b-1) e^{-\sigma_i^* j_2 t_3} \right] \right\} e^{-\sigma_i^* j_1 (t-t_3)}. \quad (15)$$

Since the higher cross-section states approach their equilibrium populations sooner than the low cross-section states, the relative population fractions of the states are altered, and $q_{\text{total } 3} = \sum_i q_{i3}$ shows a steeply decaying transient at early times as predicted by Eq. (15) and as shown in Fig. 3.

D. Repopulation and Desorption as a Function of Base Pressure

One may increase the populations at equilibrium by either decreasing the bombarding current density, j , or increasing the base pressure, P_0 , as can be seen from Eq. (10). By admitting a fixed gas leak into the system, to produce a large increase in equilibrium coverages resulting from a high base pressure, one may again change the relative population fractions. The low cross-section states will approach saturation coverages, whereas the higher cross-section states will not.

The straightforward prediction from Eqs. (11) and (12) is that in this case equilibrium desorption rates will be approached sooner and will be higher than at normal, low base pressures as shown in Fig. 4. The deviation from strict proportionality between q_e and P_0 is a measure of the decrease in sticking probability, f , as the coverage increases. For simplicity in deriving Eq. (12) it was assumed that f remains constant. With a high enough base pressure, essentially only the higher cross-section states will be active in the desorption rate decay as the equilibrium coverages of the other states will be close to saturation. One may adjust the base pressure so only the highest cross-section state is active, or the two highest, etc. This has been verified experimentally as well as a variety of other predictions based on variations of the parameters of Eq. (6). The model chosen is a simplified one, and we are aware of the many approximations inherent in it, yet it appears to represent the physical processes quite well.

E. Electron Energy Dependence

The nature of the desorption response as a function of energy is surface history dependent. In agreement with others, we found that chemically cleaned, unbaked, unbombarded surfaces would desorb gas at energies as low as 10 - 15 eV. However, after baking and electron scrubbing it was rare to see measurable desorption below 20 eV. The CO cross section peaks between 200 and 400 eV, probably depending on the relative population of the adsorbed states whose cross sections may vary differently with energy. At higher energies the desorption rate increases as subsurface gases are activated to the surface and desorbed. In order to study this effect we repopulated the "electron scrubbed" surface with CO¹⁸. The results are shown in Fig. 5. The surface adsorbed CO¹⁸ shows no high energy tail. The CO¹⁶ tail starts up at 6 keV only because extensive bombardment at 6 keV preceded the measurement. Later bombardment at 10 keV moved the tail to beyond 10 keV.

F. H₂ - CO Synergistic Adsorption

In the course of many runs it was noted that the CO adsorption-desorption character appeared to be influenced by the amount of gas phase H₂ present during adsorption. To investigate this effect we first examined the transient response under conditions of constant CO leak-in, wherein equilibrium desorption could be quickly established. With CO pressures in the 10⁻⁹ torr range, transient decays were run and reproduced with only the hydrogen ambient (2 - 3 × 10⁻¹¹ torr) present. The hydrogen pressure was then increased by adding H₂ to the CO influx.

Figure 6 shows the effect of hydrogen partial pressure on the nature of the CO response when electron bombardment is cut off for a time and then resumed. This effect was found to depend primarily on the presence of hydrogen during or before CO repopulation. The presence or absence of high H₂ partial pressures during bombardment

has little influence on the nature of the transient decay. Figure 7 shows the influence of varying H₂ exposures, at constant CO exposure, on the character of the decay curve from high to low CO desorption rates. Coverages, cross sections and repopulation exposures are tabulated below.

Run no.	119					126				
State	1	2	3	4	5	1	2	3	4	5
$\sigma^* (10^{-20} \text{ cm}^2)$										
$n_{i0} (10^{12} \text{ molecules/cm}^2)$										
CO exposure torr · sec	2.8×10^{-2}					2.8×10^{-2}				
H ₂ exposure torr · sec	2.6×10^{-6}					1.7×10^{-2}				

It is not clear from the results to date just how H₂ enhances the adsorption of CO but the effect appears to be real.

G. Aluminum Surface

It seems worthwhile to examine our results in relation to the known and postulated character of the surface of aluminum. It is well established Hunter and Fowle (1956), Ginsberg and Wefrs (1961) that the natural oxide film formed on aluminum consists of a rectifying barrier layer typically 10 - 20 Å^o thick. On top of this barrier oxide, a thicker more or less hydrated layer of γ -alumina, forms. Oxide surfaces normally terminate in anions Weyl (1953) and typically chemisorb water to form hydroxyl groups in such a way as to minimize surface energy. Peri (1960), (1965), has studied the surface hydration and dehydration of γ -alumina in great detail. Using infrared and gravimetric techniques, Peri found the extent of surface hydration dependent upon the vacuum drying temperature and time with some surface hydroxyl groups persisting to high temperatures. Five separate hydroxyl absorption bands were measured.

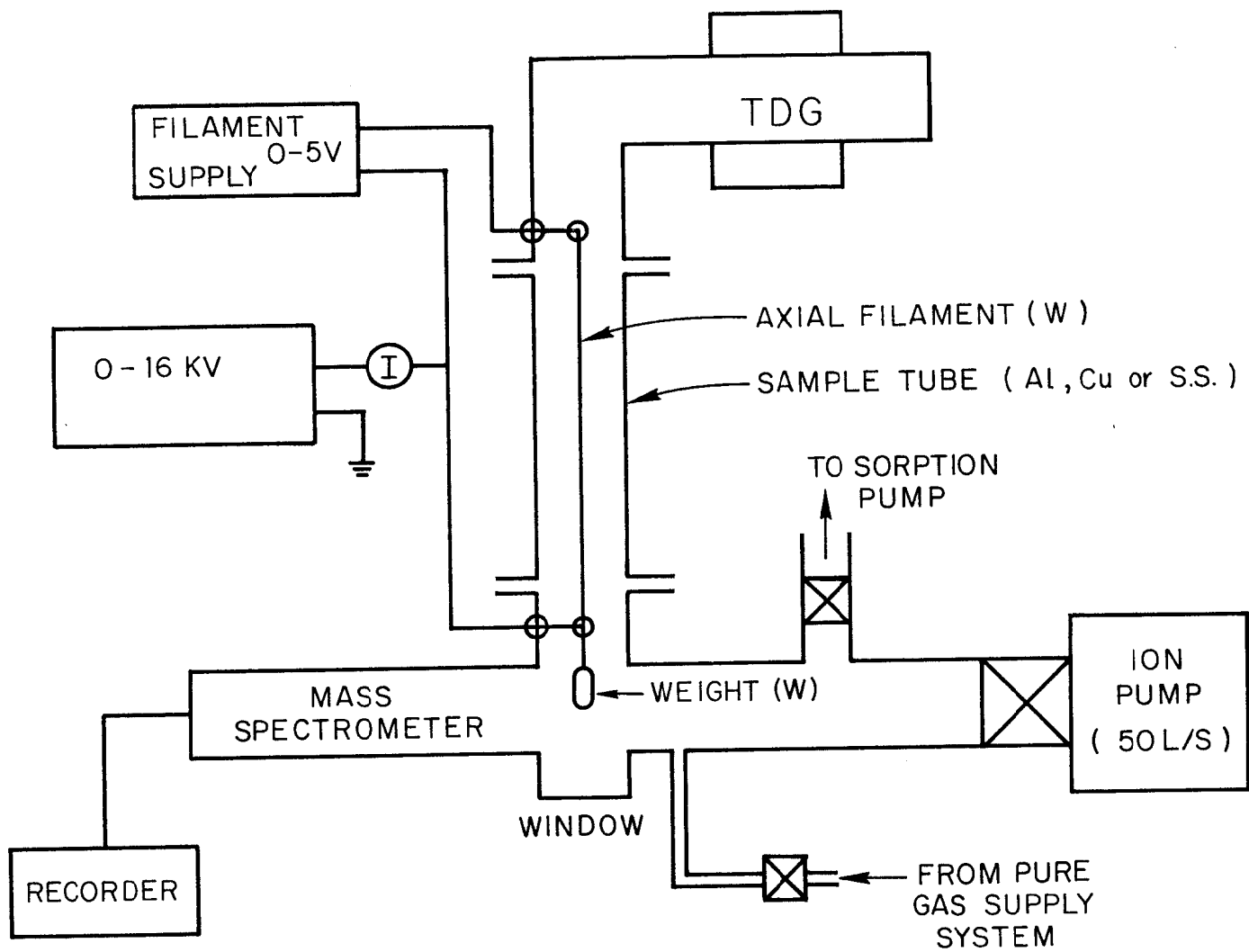
In a companion paper, Peri (1965) proposes a model for the surface of γ -alumina. Using a Monte Carlo computation technique to remove adjacent hydroxyl ions as water, the model leaves about 10% of the surface covered with five types of hydroxyl ions, differing in nearest neighbor configuration. Peri assigns these isolated hydroxyl ions to the measured infrared absorption bands. It is tempting to try to adapt this picture of the aluminum surface to our own independently derived five-state adsorption model. If we assume that CO is preferentially chemisorbed in association with hydroxyl ion sites, we can account for the low total CO coverages ($2 - 6 \times 10^{13}$ CO/cm²) and the adsorption enhancement due to added H₂*

References

- BERNARDINI, M., and MALTER, L., 1965, *J. Vac. Sci. Technol.*, 2, No. 3, 130-141.
- CLAUSING, R. E., 1965, ORNL-TM-1166.
- DEGRAS, D. A., 1962, Proc. Symp. Elect. and Vac. Physics, Hungary.
- DEGRAS, D. A., PETERMANN, L. A., and SCHRAM, A., 1962, National Symposium Vacuum Technology Trans. 9, 497.
- FISCHER, G. E., and MACK, R. A., 1965, *J. Vac. Sci. Technol.*, 2, No. 3, 123-130.
- GINSBERG, Von H., and WEFERS, K., 1961, Aluminum, Vol. 37.
- HUNTER, M. S., and FOWLE, P., 1956, *Journal of the Electrochemical Soc.*, 103, No. 9, 482-485.
- LICHTMAN, D., and McQUISTAN, R. B., 1965, Progress in Nuclear Energy, Series IX, Analytical Chemistry, 4 (Part 2), Pergamon Press.
- MOORE, G. E., and HUGHES, W. T., 1955, *Phys. Rev.* 99, 1643.
- O'NEILL, Gerard K., 1966, *Scientific American* 215, No. 5, 107.
- PERI, J. B., and HANNAN, R. B., 1960, *Journal of Phys. Chem.* 64, 1526-1530.
- PERI, J. B., 1965, *Journal of Phys. Chem.* 69, No. 1, 211-219.
- PERI, J. B., 1965, *Journal of Phys. Chem.* 69, No. 1, 220-230.
- PETERMANN, L. A., 1963, N. 2 Supplemento al Nuovo Cimento Serie I, Vol. I, 601.
- PLUMLEE, R. H., and SMITH, L. P., 1950, *J. Appl. Phys.*, 21, 811.
- REDHEAD, P. A., 1964, *Can. J. Phys.*, 42, 886.
-
- SLAC STAFF, 1966, "Proposal for a High-Energy Electron-Positron Colliding-Beam Storage Ring at the Stanford Linear Accelerator Center," Stanford University, Stanford, California.
- WEYL, W. A., 1953, Structure and Properties of Solid Surfaces (University of Chicago Press); p. 147.

Figure Captions

1. Diode desorption system schematic
2. Gas spectra
3. Transient response following repopulation at reduced bombardment
4. Effect of base pressure on equilibrium electron desorption
5. Surface and bulk electron desorption energy dependence
6. Effect of H₂ on CO adsorption-electron desorption
7. CO electron desorption decay following varying H₂ exposure at constant CO exposure



744A1

FIG.1 -- DIODE DESORPTION SYSTEM

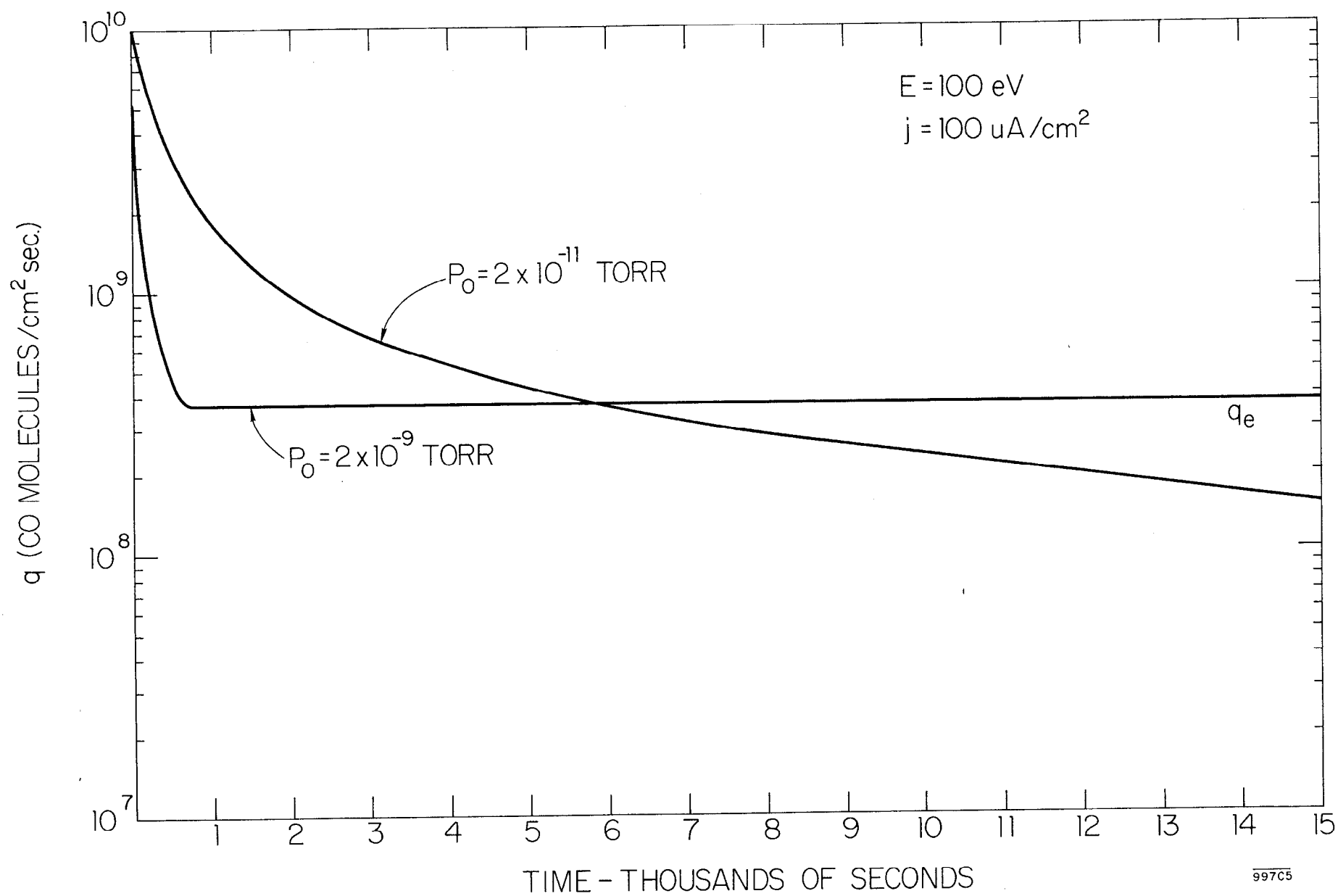


FIG. 3

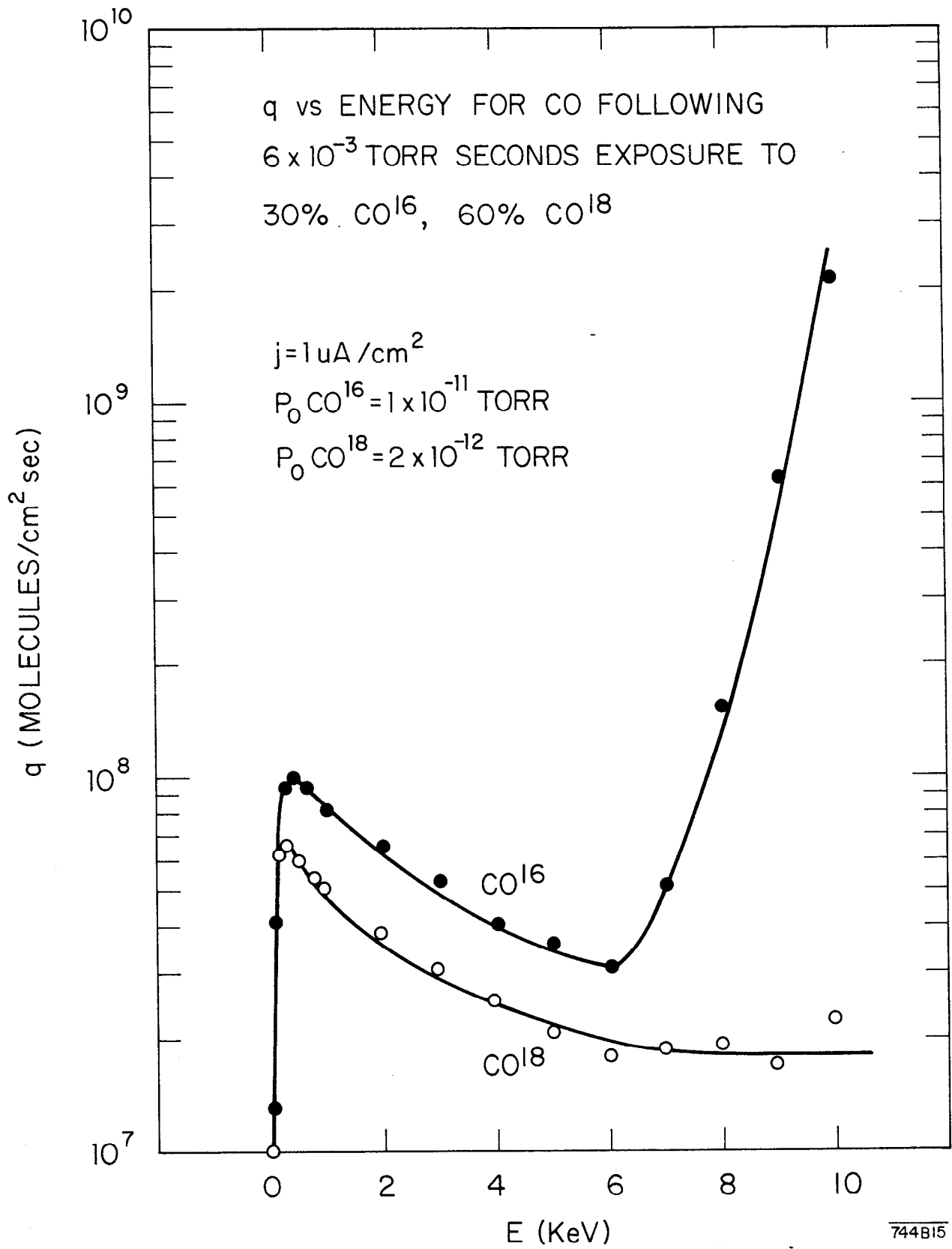


FIG. 4

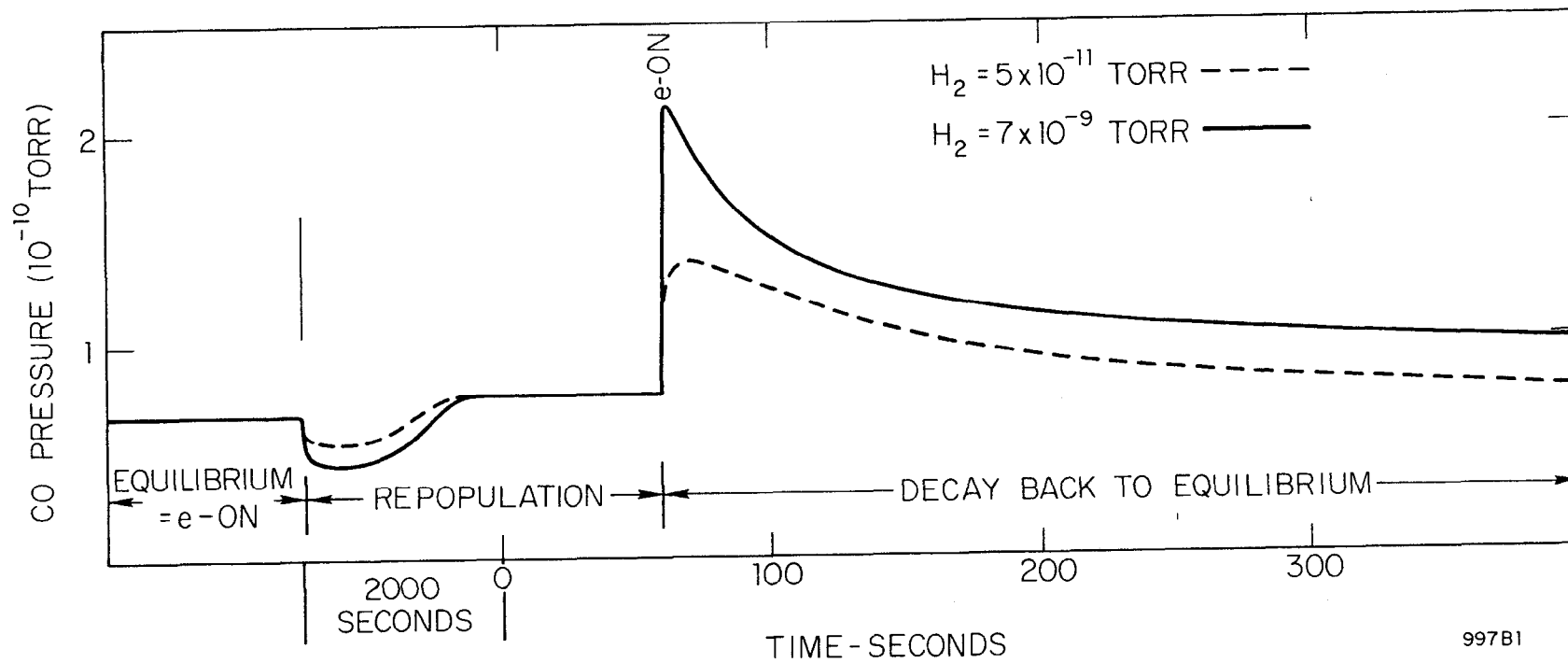


FIG. 5

997B1

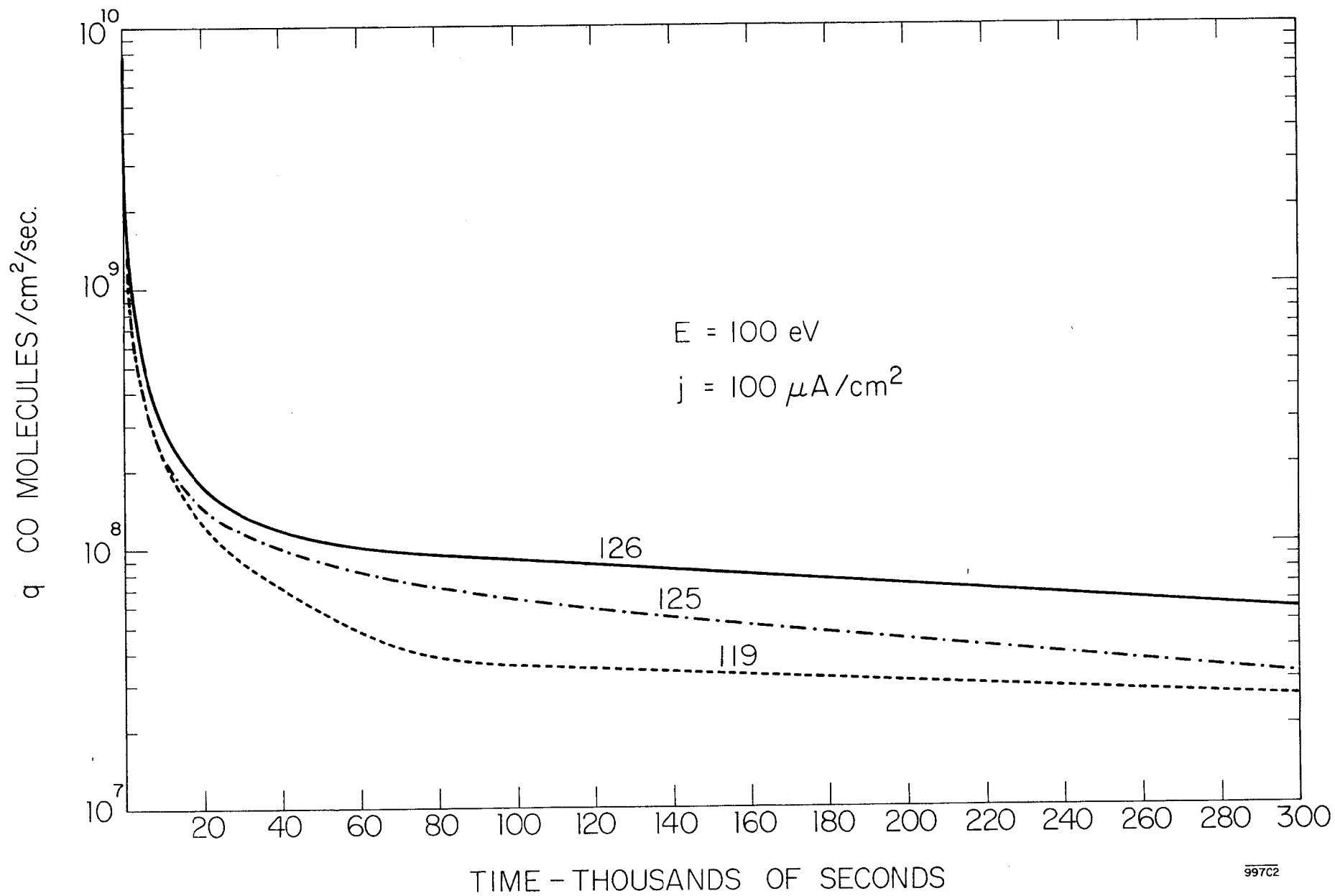


FIG. 6